Classification of Copper Alloys Microstructure using Image Processing and Neural Network

Ossama B. Abouelatta

Production Engineering and Mechanical Design Department, Faculty of Engineering, Mansoura University, 35516 Mansoura, Egypt
abouelatta@mans.edu.eg

Abstract: The most important aspect of any engineering material is its structure. The methods used to accurately determine the material microstructures is a very time-consuming process, causes operator fatigue, and it is prone to human errors and inconsistency. There are two computational approaches, a feature features and a neural network algorithm, are used separately for classifying and detection of surface textures in the field of remote sensing, science, medicine, journalism, advertising, design, education and entertainment. In this paper, a combination of the two approaches has been utilized to classify and to detect copper and copper alloys microstructure using image process, texture features and neural network. The overall average discrimination rate results from the combined approaches are about 97.6%. This paper offers a reliable basis for the classification and characterization of microscopic images by image processing and neural network.
[Ossama B. Abouelatta. **Classification of Copper Alloys Microstructure using Image Processing and Neural Network.** *J Am Sci* 2013;9(6):213-223]. (ISSN: 1545-1003). http://www.jofamericanscience.org. 25

Key words: Classification, Copper alloys, Microstructure, Image processing, Texture feature, Neural network

1 Introduction

The structure of a material is related to its composition, properties, processing history and performance. Therefore, studying the microstructure of a material provides information linking its composition and processing to its properties and performance. Recent researches towards development of a tool for detailed microstructure classification were studied by many researchers [1-9]. The main focus is put on microscale behavior, where advantages of digital material representation can be taken into account. Digital material representation allows classification of microstructures using image processing and neural network tools in an explicit manner. Incorporation of these digital microstructures into the numerical simulation methods provides the possibility to improve the quality of classification results.

A computational methodology was proposed by Tschopp *et al.* [1], for automated detection and 3D characterization of dendrite cores from images taken from slices of a production turbine blade made of a heat-treated single crystal Ni-based super-alloy. A method has been developed by Horovistiz *et al.*[2], to obtain quantitative information about grain size and shape from fractured surfaces of ceramic materials. One elaborated a routine to split intergranular and transgranular grains facets of ceramic fracture surfaces by digital image processing. Madej *et al.*[3] proposed two methods to provide an exact and statistical representation of the real microstructure which are used as input data for the finite element analysis of the micro scale compression test. Two computational intelligence approaches, a fuzzy logic algorithm and a neural network algorithm, for grain boundary detection in images of superalloy steel microstructure during sintering ware presented by Dengiz *et al.*[4]. An attempt has been made by Venkataraman *et al.*[5], with image analysis to establish the individual constituent features of the complicated as sprayed microstructure. Statistical techniques such as correlation and discriminant analysis were also used to group the microstructural features based on the process parameters.

A metallographic method for preparing samples produced by thermal barrier coatings and evaluating with the metallographic technique and digital image analysis for columnar grain size and relative intercolumnar porosity was proposed by Kelly *et al.*[6].A technique utilizing X-ray computed tomography for estimation of the orientation distribution of the fibers and pores with arbitrary shapes was developed by Dietrich *et al.*[7]. A methodology based on the processing of microstructure images with subsequent numerical simulation of the coating growth around the fibers is proposed for estimation of the local thickness of the coating. A series of image processing technologies and geometric measurement methods is introduced by Liu *et al.*[8], to quantify multiple scale microporosity in images. With the application of these methods, various basic geometric parameters of the pores can be computed automatically in the computer, such as area, perimeter, direction etc.

A methodology has been proposed by Zhang *et al.* [9], for statistical characterization of transport behavior of a typical random fibrous medium. For any given digital images of fabric sample, statistical description of the random microstructure is employed

to evaluate the permeability field, in the framework of the statistical continuum approach.

In addition, methods to analyze the texture of images such as fractional Brownian motion, box counting, and fractal dimension estimation from frequency domain, were used to numerically describe the surfaces of foods and the microstructure of potato cells, Quevedo *et al.*[10]. The image analysis method of Fourier shape description was implemented by Lorén *et al.*[11], to analyze shaped food microstructural entities, independent of their complexity, because entity shape is an important and nearly unexploited possibility for designing food material properties.

On the other hands, the microstructures of natural minerals provide information about their complex geological history. The key paradigm of digital rock physics ‘‘image and compute’’ implies imaging and digitizing the pore space and mineral matrix of natural rock and then numerically simulating various physical processes in this digital object to obtain such macroscopic rock properties as permeability, electrical conductivity, and elastic moduli, Andrä *et al.*[12]. The steps of this process include image acquisition, image processing (noise reduction, smoothing, and segmentation); setting up the numerical experiment (object size and resolution as well as the boundary conditions); and numerically solving the field equations. Yue *et al.*[13] presented a digital image processing based finite element method for the two-dimensional mechanical analysis of geomaterials by actually taking into account their material inhomogeneities and microstructures. Use of the scanning electron microscope with X-ray microanalysis allows study of clinker and cements; permitting measuring bulk phase abundance and surface areas of the phases, as well as bulk chemistry of constituent phases can be carried out, Stutzman [14].

Recently, image processing techniques are widely used in several medical areas for image improvement in earlier detection and treatment stages, where the time factor is very important to discover the abnormality issues in target images, especially in various cancer tumors such as lung cancer, breast cancer, etc. Cancer detection in magnetic resonance images is important in medical diagnosis because it provides information associated to anatomical structures as well as potential abnormal tissues necessary to treatment planning and patient follow-up. Brain cancer detection and classification system has been designed and developed by Kothari [15]. The system uses computer based procedures to detect tumor blocks or lesions and classify the type of tumor using artificial neural network in magnetic resonance images of different patients with Astrocytoma type of brain tumors. After segmentation principles, an enhanced region of the object of interest that is used as a basic foundation of feature extraction is obtained by Al-Tarawneh [16]. Relying on general features, the main detected features for accurate images comparison are pixels percentage and mask-labeling.

This paper aims to provide an automatic system to classify the microstructure of copper alloys using image processing, texture feature and neural network. This technique could be useful to in the field of image analysis applications from biomedical to remote sensing techniques.

2 Microstructure

A microstructure is the way a material comes together on a very small scale. The object’s microstructure determines the majority of its physical properties. There are four main categories that materials fall into based on their microstructure: ceramic, metallic, polymeric and composite. When describing the structure of a material, we make a clear distinction between its crystal structure and its microstructure. The term ‘crystal structure’ is used to describe the average positions of atoms within the unit cell, and is completely specified by the lattice type and the fractional coordinates of the atoms. The term ‘microstructure’ is used to describe the appearance of the material on the nm-cm length scale. Microstructure can be observed using a range of microscopy techniques .

The microstructural features of a given material may vary greatly when observed at different length scales. For this reason, it is crucial to consider the length scale of the observations you are making when describing the microstructure of a material. Microstructures are almost always generated when a material undergoes a phase transformation brought about by changing temperature and/or pressure (e.g. a melt crystallizing to a solid on cooling).

Macrostructural and microstructural examination techniques are employed in areas such as routine quality control, failure analysis and research studies. In quality control, microstructural analysis is used to determine if the structural parameters are within certain specifications. It is used as a criterion for acceptance or rejection. Various techniques for quantifying microstructural features, such as grain size, particle or pore size, volume fraction of a constituent, and inclusion rating, are available for comparative analysis.

3 Image Processing and Texture Features

Today, image analysis with the aid of computer, becomes more and more substantial in all research fields. Image analysis involves investigation of the image data for a specific application. Normally, the raw data of a set of images is analyzed to gain insight

into what is happening with the images and how they can be used to extract desired information.

3.1 Texture Features

Texture is visual patterns with properties of homogeneity that do not result from the presence of only a single color such as clouds and water [17]. There are many techniques to measure texture similarity, the best-established rely on comparing values of what are known as second-order statistics calculated from query and stored images. Essentially, they calculate the relative brightness of selected pairs of pixels from each image. From these, it is possible to calculate measures of image texture such as the degree of contrast, coarseness, directionality and regularity [18], or periodicity, directionality and randomness [19]. Alternative methods of texture analysis for retrieval include the use of Gabor filters [20] and fractals [21]. Visual textures refer to the visual impression that textures produce to human observer, which are related to local spatial variations of simple stimuli like color, orientation and intensity in an image. The image analysis involves image segmentation, image transformation, pattern classification, feature extraction, texture synthesis and shape from texture [22]. Table 1 lists the most important image processes and analysis.

3.2 GLCM and Haralick Texture Features

In 1973, Haralick [23] introduced the co-occurrence matrix and its texture features which are the most popular second order statistical features today. Haralick proposed two steps for texture feature extraction: the first is computing the co-occurrence matrix and the second step is calculating texture feature base on the co-occurrence matrix. This technique is useful in wide range of image analysis applications from biomedical to remote sensing techniques. The Grey level co-occurrence matrix (GLCM) is defined as:

$$G(i,j) = P(i,j) / \sum_{i=0}^{n} \sum_{j=0}^{n} P(i,j)$$

One of the defining qualities of texture is the spatial distribution of gray values. The use of statistical features is therefore one of the early methods proposed in the image processing literature. Haralick suggested the use of co-occurrence matrix or gray level co-occurrence matrix. It considers the relationship between two neighboring pixels, the first pixel is known as a reference and the second is known as a neighbor pixel. Haralick extracted thirteen texture features from GLCM for an image. These features are extended to 22 texture features, Table 2.

Table 1: Classification of image analysis.

No.	Process	Description
1	Image segmentation	It divides the input image into multiple segments or regions, which show objects or meaningful parts of objects. It segments image into homogeneous regions thus making it easier to analyze them.
2	Image transformation	It is used to find the spatial frequency information that can be used in the feature extraction step.
3	Pattern classification	It aims to classify data (patterns) based either on a priori knowledge or on statistical information extracted from the image.
4	Feature extraction	It is the process of acquiring higher level information of an image, such as color, shape, and texture. Features contain the relevant information of an image and will be used in image processing.
5	Texture synthesis	It is a common technique to create large textures from usually small texture samples, for the use of texture mapping in surface or scene rendering applications.
6	Shape from texture	It reconstructs 3D surface geometry from texture information.

4 Neural Networks [24]

ANNs apply the principle of function approximation by example, meaning that they learn a function by looking at examples of this function. One of the simplest examples is an ANN learning the XOR function, but it could just as easily be learning to determine the language of a text, or whether there is a tumor visible in an X-ray image. If an ANN is to be able to learn a problem, it must be defined as a function with a set of input and output variables supported by examples of how this function should work. A problem like the XOR function is already defined as a function with two binary input variables and a binary output variable, and with the examples which are defined by the results of four different input patterns.

However, there are more complicated problems which can be more difficult to define as functions. The input variables to the problem of finding a tumor in an X-ray image could be the pixel values of the image, but they could also be some values extracted from the image. The output could then either be a binary value or a floating point value representing the probability of a tumor in the image. In ANNs this floating-point value would normally be between 0 and 1, inclusive.

Table 2: Texture features parameters

No.	Definition	Formula
1	***Contrast (CON)*** Contrast is a measure of the amount of local variation in the image. A low value results from uniform images (if the grey levels of each pixel pair are similar) whereas images with greater variation produce a high value.	$CON = \sum_{i=0}^{n-1} n^2 \sum_{j=0}^{n-1} G(i,j)(i-j)^2$
2	***Dissimilarity (DIS)*** Dissimilarity is similar to the contrast. It will be high when the local region has a high contrast. This feature is sensitive to both grey level spatial variability and tone of the input image.	$DIS = \sum_{i=0}^{n-1}\sum_{j=0}^{n-1} G(i,j)\lvert i-j\rvert$
3	***Homogeneity HOM/inverse difference moment (IDM)*** The homogeneity (or inverse difference moment) is expected to be large if the grey levels of each pixel pair are similar. This occurs when the image is locally homogeneous in the scale of the length of spatial.	$HOM = \sum_{i=0}^{n-1}\sum_{j=0}^{n-1} \frac{G(i,j)}{1+(i-j)^2}$
4	***Similarity (SIM)*** Similarity is a first-degree measure of homogeneity.	$SIM = \sum_{i=0}^{n-1}\sum_{j=0}^{n-1} \frac{G(i,j)}{1+\lvert i-j\rvert}$
5	***Angular second moment (ASM)*** ASM is a measure of the homogeneity of an image. ASM is sometimes defined as energy or uniformity and it can be considered as the opposite of entropy. This feature is sensitive to the grey level of homogeneity within the texture field.	$ASM = \sum_{i=0}^{n-1}\sum_{j=0}^{n-1} G(i,j)^2$
6	***Entropy (ENT)*** Entropy measures the randomness of a grey level distribution. It is expected to be high if the grey levels are distributed randomly throughout the image. For homogeneous or simple patterned data, Entropy is very small, i.e. inhomogeneous scenes have low order entropy, while a homogeneous scene has high entropy.	$ENT = -\sum_{i=0}^{n-1}\sum_{j=0}^{n-1} G(i,j).\ln[G(i,j)]$
7	***Mean (sum mean) (μ)*** The GLCM mean is not simply the average of all the original pixel values in the image. It is expressed in terms of the GLCM. The pixel value is weighted not by its frequency of occurrence by itself (as in a regular mean equation), but by the frequency of its occurrence in combination with a certain neighbor pixel value.	$\mu = \sum_{i=0}^{n-1}\sum_{j=0}^{n-1} iG(i,j)$
8	***Variance and standard deviation (VAR and SD)*** Variance tells how spread out the distribution of grey levels is. The variance is expected to be large if the grey levels of the image are spread out greatly. Variance uses the GLCM, not the greys in the original images.	$VAR = \sum_{i=0}^{n-1}\sum_{j=0}^{n-1} G(i,j)(i-\mu_x)^2$ where $\mu_x = \sum_{i=0}^{n-1} i \sum_{j=0}^{n-1} G(i,j)$
9	***Maximum probability (MaxP)*** The maximum probability calculates grey-level, which has the maximum probability in the GLCM. It is expected to be high if the occurrence of the most predominant pixel pairs is high.	$MaxP = max_i^m max_j^n G(i,j)$
10	***Correlation (COR)*** Correlation is a measure of grey level linear dependence between the pixels at the specified positions relative to each other. When the scale of local texture is much larger than the distance of spatial, correlation is typically high and vice versa.	$COR = \sum_{i=0}^{n-1}\sum_{j=0}^{n-1} \frac{G(i,j)[(i-\mu_x)(j-\mu_y)]}{\sigma_x\sigma_y}$ where μ_y is the mean for every column, σ_x is the standard deviation for every row, and σ_y is the standard deviation for every column.
11	***Diagonal moment (DM)*** The *DM* measures the differences in correlation for high and low grey levels.	$DM = \sum_{i=0}^{n-1} j \sum_{j=0}^{n-1} (0.5\ G(i,j)\lvert i-j\rvert)^{0.5}$
12	***Second diagonal moment (SDM)*** The *SDM* measures the second moment of the differences in correlation for high and low grey levels.	$SDM = \sum_{i=0}^{n-1} j \sum_{j=0}^{n-1} (0.5\ G(i,j)\lvert i-j\rvert)$

13	***Coefficient of variation (CVAR)*** The coefficient of variation is a measure of the dispersion of grey level transitions calculated in relation to the average value.	$CVAR = \frac{\sigma}{\mu}$
14	***Sum entropy (SENT)*** The sum entropy is a measure of the sum of micro (local) differences in an image.	$SENT = -\sum_{i=2}^{2n} G_{x+y}(i)\ln[G_{x+y}(i)]$
15	***Sum variance (SVAR)*** The sum variance reveals spatial heterogeneity (dissimilarity) of an image.	$SVAR = -\sum_{i=2}^{2n} G_{x+y}(i)(\mathrm{i} - \mathrm{SENT})^2$
16	***Difference entropy (DENT)*** The difference entropy is a measure of the variability of micro (local) differences.	$DENT = -\sum_{i=0}^{n-1} G_{x-y}(i)\ln[G_{x-y}(i)]$
17	***Difference variance (DVAR)*** The difference variance is a measure of the local variability.	$DVAR = -\sum_{i=0}^{n-1} G_{x-y}(i)(\mathrm{i} - \mathrm{DENT})^2$
18	***Cluster shade (CSH)*** The cluster shade is a two-dimensional version of the gray-level histogram skewness, which is a measure of the degree of asymmetry of a distribution.	$CSH = -\sum_{i=0}^{n-1}\sum_{j=0}^{n-1} G(i,j)[(i+j) - (\mu_x + \mu_y)]^3$
19	***Cluster prominence (CPR)*** The cluster prominence is a two-dimensional version of the gray-level histogram kurtosis, which is a measure of how peaked is a distribution.	$CPR = -\sum_{i=0}^{n-1}\sum_{j=0}^{n-1} G(i,j)[(i+j) - (\mu_x + \mu_y)]^4$
20	***Sum average (SAVR)*** The sum average is a measure of the relation between clear and dense areas in an image.	$SAVR = \sum_{i=0}^{n-1} iG_{x+y}(i)$ where $G_{x+y}(i+j) = \sum_{i=0}^{n-1}\sum_{j=0}^{n-1} G(i,j)$
21	***Mean correlation 1 (MCOR1)*** The mean correlation 1 feature is also known as information measure. In this feature, two derived arrays from the GLCM must be used. The first array represents the summation of rows in the GLCM, while the second array represents the summation of columns.	$MCOR1 = \frac{ENT - HXY1}{\max(HX, HY)}$ where $HXY1 = -\sum_{i=0}^{n-1}\sum_{j=0}^{n-1} G(i,j)\ln[G_x(i), G_y(j)]$ $G_x(i) = \sum_{j=0}^{n-1} G(i,j)$ $G_y(i) = \sum_{i=0}^{n-1} G(i,j)$ *HX* and *HY* are the entropies of $P_x(i)$ and $P_y(j)$, respectively.
22	***Mean correlation 2 (MCOR2)*** This is another form for calculating the mean correlation.	$MCOR2 = \sqrt{1 - exp^{-2(HXY2 - ENT)}}$ where $HXY2 = \sum_{i=0}^{n-1}\sum_{j=0}^{n-1} G_x(i)G_y(j)\ln[G_x(i)G_y(j)]$

G is the normalized GLCM, i, j are the row and column of each element in the GLCM and n is the number of the GLCM elements, then the following texture features can be calculated from the GLCM.

4.1 Texture Features

Basic knowledge of how the human brain operates is needed to understand how ANNs work. The human brain is a highly complicated system which is capable to solve very complex problems, Fig. 1 (a). The brain consists of many different elements, but one of its most important building blocks is the neuron, of which it contains approximately 1011. These neurons are connected by around 1015 connections, creating a huge neural

network. Neurons send impulses to each other through the connections and these impulses make the brain work. The neural network also receives impulses from the five senses and sends out impulses to muscles to achieve motion or speech. The individual neuron can be seen as an input/output machine which waits for impulses from the surrounding neurons and, when it has received enough impulses, it sends out an impulse to other neurons.

(a)The human brain

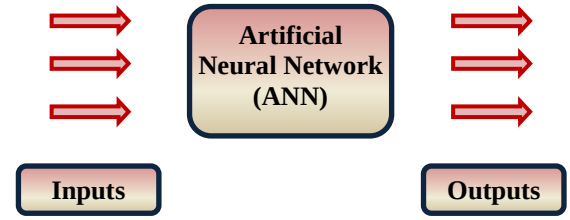

(b)The neural network

Fig. 1. Basic knowledge of ANN.

4.2Artificial Neural Networks

Artificial neurons are similar to their biological counterparts, Fig. 1 (b). They have input connections which are summed together to determine the strength of their output, which is the result of the sum being fed into an activation function [25]. Though many activation functions exist, the most common is the sigmoid activation function, which outputs a number between 0 (for low input values) and 1 (for high input values). The resultant of this function is then passed as the input to other neurons through more connections, each of which are weighted. These weights determine the behavior of the network. In the human brain the neurons are connected in a seemingly random order and send impulses asynchronously. If we wanted to model a brain this might be the way to organize an ANN, but since we primarily want to create a function approximator, ANNs are usually not organized like this [26].

When we create ANNs, the neurons are usually ordered in layers with connections going between the layers. The first layer contains the input neurons and the last layer contains the output neurons. These input and output neurons represent the input and output variables of the function that we want to approximate. Between the input and the output layer a number of hidden layers exist and the connections (and weights) to and from these hidden layers determine how well the ANN performs. When an ANN is learning to approximate a function, it is shown examples of how the function works and the internal weights in the ANN are slowly adjusted so as to produce the same output as in the examples. The hope is that when the ANN is shown a new set of input variables, it will give a correct output. Therefore, if an ANN is expected to learn to spot a tumor in an X-ray image, it will be shown many X-ray images containing tumors, and many X-ray images containing healthy tissues. After a period of training with these images, the weights in the ANN should hopefully contain information which will allow it to positively identify tumors in X-ray images that it has not seen during the training.

ANNs are machine learning programs based on neuron like building blocks similar to the neurons in the human brain, Fig. 2. Most of the research and applications of neural networks involves feed-forward networks trained by the back-propagation algorithm. These ANNs usually undergo a training phase by feeding it a set of inputs with known outcome, and then back-propagating the known results to adjust the weights among the neural elements. After many iterations of training, called epochs, the NN is able to detect subtle patterns in large data sets and make predictions based on what it has learned through past observations. Feed forward neural network architecture was selected based on the flexibility and applicability of the approach in a variety of problems.

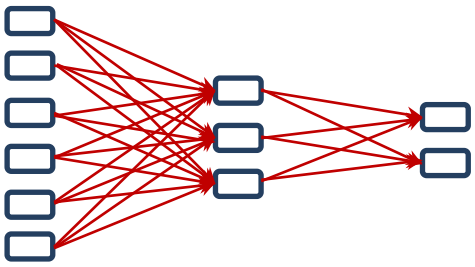

Fig. 2. An ANN with six input neurons, a hidden layer and two output neurons.

5. Material and Methods

Interpretation of microstructures requires an understanding of the processes by which various structures are formed. Microstructural features, such as grain size, inclusions, impurities, second phases, porosity, segregation or surface effects, are a function of the starting material and subsequent processing treatments. Microstructural analysis is used in research studies to determine the microstructural

changes that occur as a result of varying parameters such as composition, heat treatment or processing steps.

According to Fig. 3, the following procedures were applied to classify copper alloys microstructure using image processing, texture feature and neural network as:

1. Eighteen cases of copper and copper alloys were collected in order to apply the proposed method of microstructure classification [27]. These cases are illustrated in Fig. 4.
2. Each image has the same size which is 768×512 pixels. Each image was divided into 7 images (5 were used for training and 2 for validation). Each one of the new image has a size of 100×100 pixels.
3. Each image was converted to gray scale image. Twenty two texture features were calculated and stored in a file to be used as input data, Table 3. The input dataset is an array of 90×22 (90 image × 22 texture feature parameter).
4. The output array was created so as each case was represented in one row. For example, case one 'Aluminum bronze, 6-7.5Al(C61300)'is defined as: [1 0 0 0 0 0 0 0 0 0 0 0 0 0 0 0 0 0]. The output dataset is an array of 90×18 (90 image × 18 case) as follows:

$$T = \begin{bmatrix} 1 & 0 & 0 & 0 & .. & .. & .. & .. & 0 \\ 1 & 0 & 0 & 0 & .. & .. & .. & .. & 0 \\ .. & .. & & .. & .. & & .. & .. & \\ .. & .. & & .. & .. & & .. & .. & \\ 0 & 1 & 0 & 0 & .. & .. & .. & .. & 0 \\ 0 & 1 & 0 & 0 & .. & .. & .. & .. & 0 \\ .. & .. & & .. & .. & & .. & .. & \\ .. & .. & & .. & .. & & .. & .. & \\ 0 & 0 & 0 & 0 & .. & .. & .. & .. & 1 \end{bmatrix}$$

5. A feed forward neural network with error back propagation algorithm was adopted for the NN system. Here it is used to classify copper alloys microstructure through microstructure images.
6. Input/output datasets were used to train the network. A procedure was employed to optimize the hidden layer neurons and select the transfer function for which a program was generated in MATLAB software.
7. About 100 training process were performed and the best net was extracted and saved for later use. The best net was selected as the results of its output have the heist percentage value of successful prediction.
8. A program was built especially for the classification of microstructure named Microstructure Classification Program "*MSCProg*". This program was built using Matlab Software Packages. Fig. 5 (a) shows the main interface of the program and Fig. 5 (b) shows the details of microstructure.

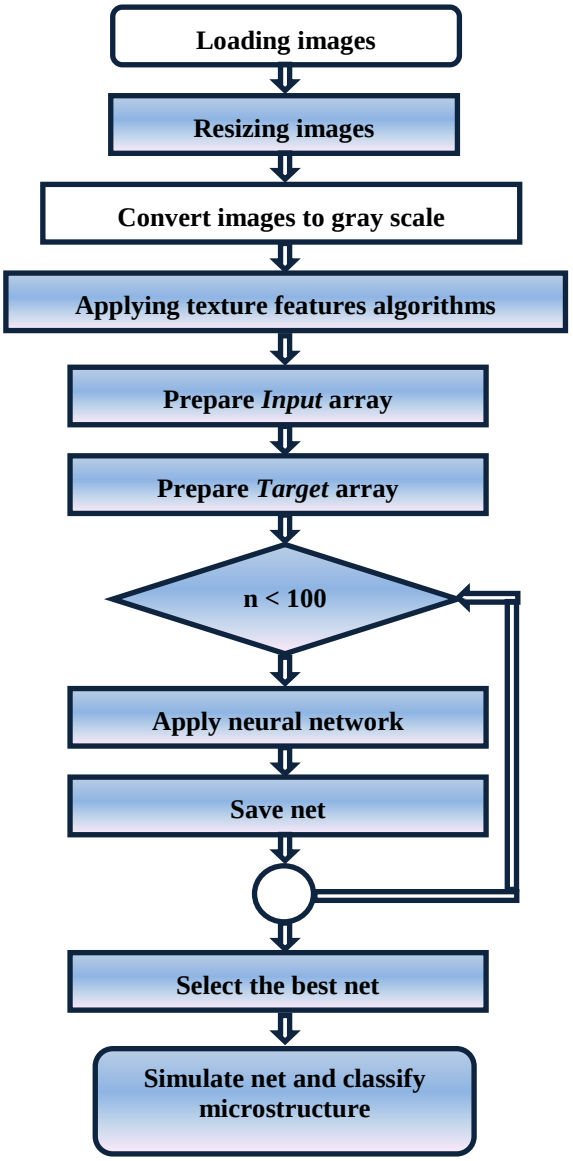

Fig. 3. Block diagram of microstructure classification of copper and copper alloys.

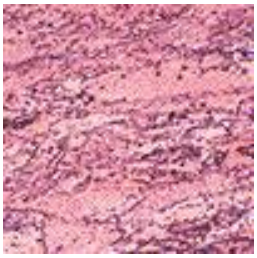
(1) Aluminum bronze, 6-7.5 Al (C61300)

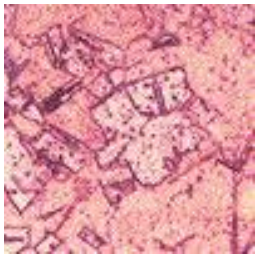
(2) Aluminum bronze, 6-7.5 Al (C61300)

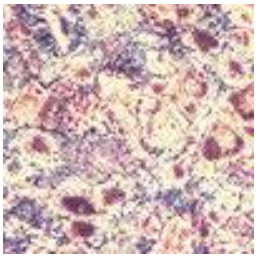
(3) Nickel-aluminum bronze, 9.0-11.0 Al, 4.0-5.5 Ni (C63000)


(4) Guilding, 95% (C21000)


(5) Commercial bronze, 90% (C22000)

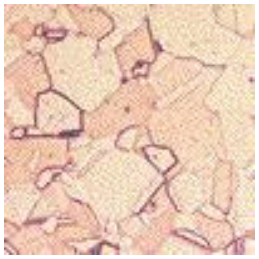
(6) Cartridge brass, 70% (C26000)

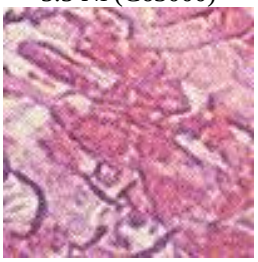
(7) Cadmium copper (C16200)


(8) Cadmium copper (C16200)

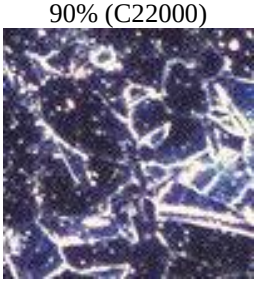
(9) Cadmium copper (C16500)

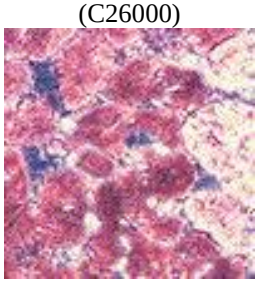
(10) Copper-5 Ni-2.5 Ti


(11) Copper-nickel, 10% (C70600)


(12) ETP (C11000)


(13) High leaded tin bronze, 6-8 Pb (C93200)


(14) Medium leaded brass, 62% (C35000)

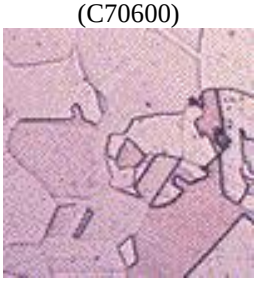
(15) Nickel-silver, 72-18 (C73500)

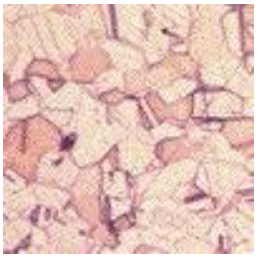
(16) Nickel-silver, 59-12 (C76200)

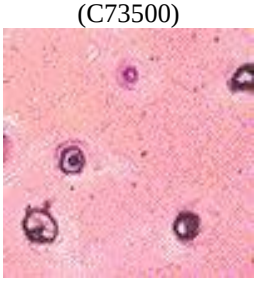
(17) Phosphor bronze, 1.25% E (C50500)


(18) Phosphor bronze, 1.25% E (C50500)

Fig. 4. Eighteen cases of copper and copper alloy's microstructure.

Table 3: Classification of image analysis.

No.	Texture features	Value
1	Autocorrelation (AUTOC)	26.93347
2	Contrast (CONTR)	1.27684
3	Correlation (CORRM)	0.41265
4	Correlation (CORRP)	0.41265
5	Cluster Prominence (CPROM)	27.94876
6	Cluster Shade (CSHAD)	-2.61098
7	Dissimilarity (DISSI)	0.79622
8	Energy (ENERG)	0.09638
9	Entropy (ENTRO)	2.70866
10	Homogeneity (HOMOM)	0.67090
11	Homogeneity (HOMOP)	0.64941
12	Maximum probability (MAXPR)	0.17622
13	Sum of squares - Variance (SOSVH)	27.30146
14	Sum average (SAVGH)	10.29276
15	Sum variance (SVARH)	72.73104
16	Sum entropy (SENTH)	1.94643
17	Difference variance (DVARH)	1.27684
18	Difference entropy (DENTH)	1.11464
19	Info. measure of correlation (1) (INF1H)	-0.07479
20	Info. measure of correlation (2) (INF2H)	0.43626
21	Inverse difference normalized (INDNC)	0.91659
22	Inverse difference moment normalized (IDMNC)	0.98135

6. Results

The results of the testing processes are shown in Table 4. The average discrimination rate shows that 15 cases can be completely classified and only 3 cases have a discrimination rate of 85.7%. This means that these three cases failed in one image from 7 images (5 for training and 2 for validation). The overall average discrimination rate is about 97.6%.

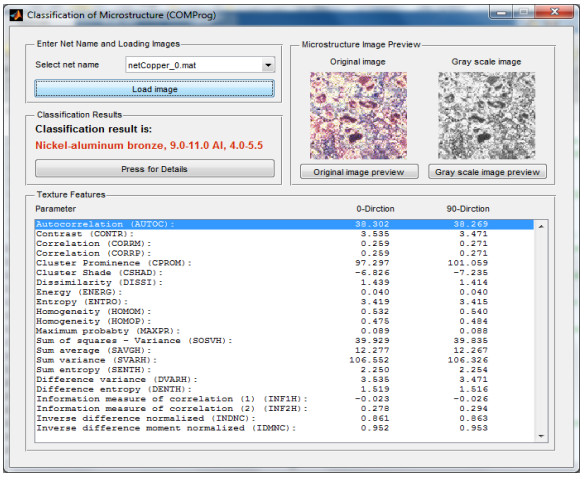

(a) Main interface of the program.

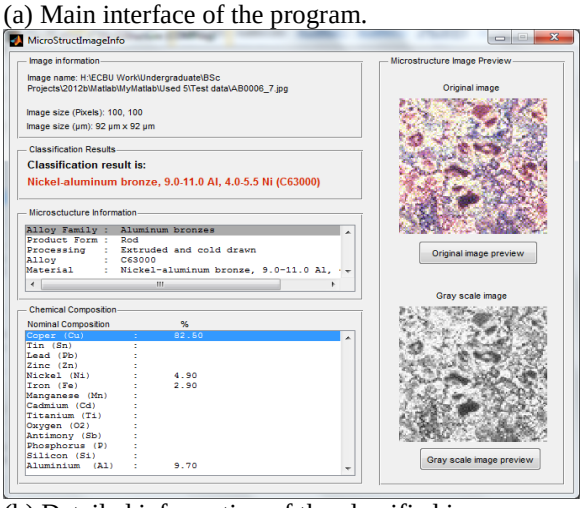

(b) Detailed information of the classified image.

Fig. 5. *MSCProg*, Microstructure Classification Program.

Table 4: Classification of image analysis.

	1	2	3	4	5	6	7	8	9	10	11	12	13	14	15	16	17	18	%
1	100	0	0	0	0	0	0	0	0	0	0	0	0	0	0	0	0	0	100
2	0	**85.7**	0	0	0	0	0	0	0	0	0	**14.3**	0	0	0	0	0	0	85.7
3	0	0	100	0	0	0	0	0	0	0	0	0	0	0	0	0	0	0	100
4	0	0	0	**85.7**	0	0	0	0	0	0	0	0	0	0	0	0	**14.3**	0	85.7
5	0	0	0	0	100	0	0	0	0	0	0	0	0	0	0	0	0	0	100
6	0	0	0	0	0	**85.7**	0	0	0	0	0	0	0	0	0	**14.3**	0	0	85.7
7	0	0	0	0	0	0	100	0	0	0	0	0	0	0	0	0	0	0	100
8	0	0	0	0	0	0	0	100	0	0	0	0	0	0	0	0	0	0	100
9	0	0	0	0	0	0	0	0	100	0	0	0	0	0	0	0	0	0	100
10	0	0	0	0	0	0	0	0	0	100	0	0	0	0	0	0	0	0	100
11	0	0	0	0	0	0	0	0	0	0	100	0	0	0	0	0	0	0	100
12	0	0	0	0	0	0	0	0	0	0	0	100	0	0	0	0	0	0	100
13	0	0	0	0	0	0	0	0	0	0	0	0	100	0	0	0	0	0	100
14	0	0	0	0	0	0	0	0	0	0	0	0	0	100	0	0	0	0	100
15	0	0	0	0	0	0	0	0	0	0	0	0	0	0	100	0	0	0	100
16	0	0	0	0	0	0	0	0	0	0	0	0	0	0	0	100	0	0	100
17	0	0	0	0	0	0	0	0	0	0	0	0	0	0	0	0	100	0	100
18	0	0	0	0	0	0	0	0	0	0	0	0	0	0	0	0	0	100	100
Average discrimination rate																			**97.62**

7. Conclusion and Recommendations

Since there is no universal approach for obtaining accurate image classification, almost all techniques use only one approach: texture features or neural network. This is way a classification based on the criterion used by each technique is almost not enough. Instead, a combination of both methods is proposed to achieve a good classification results and is helpful for better use of existing method and for improving their performance as well as for designing new ones. As a general tendency, we can conclude that a new technique use a combined texture features and neural networks were applied and seemed to provide stable and accurate classification results. The overall average discrimination rate results from the combined approaches are about 97.6%. This technique can be expanded to cover many areas of interest such as: remote sensing, medicine, science, journalism, advertising, design, education and entertainment.

Corresponding author
Ossama B. Abouelatta
Production Engineering and Mechanical Design Department, Faculty of Engineering, Mansoura University, 35516 Mansoura, Egypt.
abouelatta@mans.edu.eg

References

1. Tschopp M.A., M.A. Groeber, J.P. Simmons, A.H. Rosenberger, and C. Woodward, "Automated extraction of symmetric microstructure features in serial sectioning images," Materials Characterization, Vol. 61, pp. 1406–1417, 2010
2. Horovistiz A.L., J.R. Frade, and L.R.O. Hein, "Comparison of fracture surface and plane section analysis for ceramic grain size characterization," Journal of the European Ceramic Society, Vol. 24, pp. 619–626, 2004
3. Madej L., L. Rauch, K. Perzynski, and P. Cybulka, "Digital Material Representation as an efficient tool for strain inhomogeneities analysis at the micro scale level," Archives of Civil and Mechanical Engineering, Vol. XI, No. 3, pp. 661–679, 2011
4. Dengiz O., Alice E. Smith, and Ian Nettleship, "Grain boundary detection in microstructure images using computational intelligence," Computers in Industry, Vol. 56, pp. 854–866, 2005
5. Venkataraman R., Gautam Das, B. Venkataraman, G.V. Narashima Rao, and R. Krishnamurthy, "Image processing and statistical analysis of microstructures of as plasma sprayed Alumina–13 wt.% Titaniacoatings," Surface & Coatings Technology, Vol. 201, pp. 3691–3700, 2006
6. Kelly M., Jogender Singh, Judith Todd, Steven Copley, Douglas Wolfe, "Metallographic techniques for evaluation of Thermal Barrier Coatings produced by Electron Beam Physical Vapor Deposition," Materials characterization, Vol. 59, pp. 863–870, 2008
7. Dietrich S., J.-M. Gebert, G. Stasiuk, A. Wanner, K.A. Weidenmann, O. Deutschmann, I. Tsukrov, and R. Piat, "Microstructure characterization of CVI-densified carbon/carbon composites with various fiber distributions," Composites Science and Technology, Vol. 72, pp. 1892–1900, 2012
8. Liu C., Bin Shi, Jian Zhou, and Chaosheng Tang, "Quantification and characterization of microporosity by image processing, geometric measurement and statistical methods: Application on SEM images of clay materials," Applied Clay Science, Vol. 54, pp. 97–106, 2011
9. Zhang F., S. Comas-Cardona, C. Binetruy, "Statistical modeling of in-plane permeability of non-woven random fibrous reinforcement," Composites Science and Technology, Vol. 72, pp. 1368–1379, 2012
10. Quevedo R., López-G. Carlos, José M. Aguilera, and Laura Cadoche, "Description of food surfaces and microstructural changes using fractal image texture analysis," Journal of Food Engineering, Vol. 53, pp. 361–371, 2002
11. Lorén N., Lars Hamberg, and Anne-Marie Hermansson, "Measuring shapes for application in complex food structures," Food Hydrocolloids, Vol. 20, pp. 712–722, 2006
12. Andrä H., Nicolas Combaret, Jack Dvorkin, Erik Glatt, Junehee Han, Matthias Kabel, Youngseuk Keehm, Fabian Krzikalla, Minhui Lee, Claudio Madonna, Mike Marsh, Tapan Mukerji, Erik H. Saenger, Ratnanabha Sain, Nishank Saxena, Sarah Ricker, Andreas Wiegmann, and Xin Zhan, "Digital rock physics benchmarks—Part I: Imaging and segmentation," Computers & Geosciences, Vol. 50, pp. 25–32, 2013
13. Yue Z.Q., S. Chen, and L.G. Tham, "Finite element modeling of geomaterials using digital image processing," Computers and Geotechnics, Vol. 30, pp. 375–397, 2003
14. Stutzman P., "Scanning electron microscopy imaging of hydraulic cement microstructure," Cement & Concrete Composites, Vol. 26, pp. 957–966, 2004
15. Kothari A., "Detection and classification of brain cancer using artificial neural network in

MRI images," World Journal of Science and Technology, Vol. 2, No. 5, pp. 01-04, 2012
16. Mokhled S. Al-Tarawneh, "Lung Cancer Detection Using Image Processing Techniques," Leonardo Electronic Journal of Practices and Technologies, Vol. 20, pp. 147-158, January-June 2012
17. Smith J. R. and F. S. Chang, "Automated binary texture feature sets for image retrieval," Proc. Int. Conf. on Acoustics, Speech, and Signal Processing, pp. 2241-2246, 1996
18. Meethongjan, K. Mohamad, D., Rehman, A. Altameem, A. and Saba, T. (2013). An Intelligent Fused Approach for Face Recognition, Journal of Intelligent Systems, vol.22(1), pp. 71-80.
19. Rehman, A. and Saba, T. (2012). "Neural Network for Document Image Preprocessing: State of the Art" Artificial Intelligence Review, ,DOI: 10.1007/s10462-012-9337-z.
20. Elarbi-Boudihir, M. Rehman, A. Saba, T. (2011) Video motion perception using optimized Gabor filter, International Journal of Physical Sciences, vol. 6 (12), 2799-2806.
21. T. Saba and A.Rehman (2012). Effects of Artificially Intelligent Tools on Pattern Recognition, International Journal of Machine Learning and Cybernetics, vol. 4(2), pp. 155-162. DOI: 10.1007/s13042-012-0082-z
22. Rehman, A. Alqahtani, S. Altameem, A. Saba, T. (2013) Virtual Machine Security Challenges: Case Studies, International Journal of Machine Learning and Cybernatics, DOI 10.1007/s13042-013-0166-4.
23. Shanmugam K. R. M. Haralick and I. H. Dinstein, "Textural features for image classification," IEEE Transactions on Systems, Man and Cybernetics, Vol. 3, pp. 610-621, 1973
24. Nissen S., "Neural Networks Made Simple, Artificial Intelligence," Software 2.0 2/2005, pp. 14-19, www.software20.org
25. Saba,T. Rehman, A. and Sulong, G. (2010) "An Intelligent Approach to Image Denoising" Journal of Theoretical and Applied Information Technology, vol. 17 (1), pp. 32-36.
26. Saba, T. and Alqahtani, F.A. (2013) Semantic Analysis Based Forms Information Retrieval and Classification, 3 D Research, vol. 4(4).DOI. 10.1007/3DRes.03(2013)4.
27. Saba, T. and Rehman,A. (2012), Machine Learning and Script Recognition, Lambert Academic Publisher, pp. 87-100, ISBN-10: 3659111708.

4/29/2013